

# 北山地区早古生代洋盆俯冲记录 ——来自石板井高镁闪长岩的年代学、地球化学证据

专少鹏, 陈超, 申宗义, 潘志龙, 张运强, 赵华平, 陈宏强, 杨瑞, 修迪

(河北省区域地质调查院, 河北廊坊 065000)

**摘要:** 北山造山带中部石板井地区发育高镁闪长岩体。LA-ICP-MS 锆石 U-Pb 分析获得该类岩石的年龄为  $456 \pm 2$  Ma, 表明其形成于晚奥陶世。地球化学数据显示: 岩石属钠质钙碱性系列,  $\text{SiO}_2$  含量为 51.94% ~ 55.30%, 具有较高的  $\text{MgO}$  (4.12% ~ 6.19%, 平均 5.17%)、 $\text{Mg}^{\#}$  值 (0.45 ~ 0.69, 平均 0.53)、 $\text{Cr}$  ( $35.82 \times 10^{-6}$  ~  $985.50 \times 10^{-6}$ , 平均  $284.84 \times 10^{-6}$ )、 $\text{Ni}$  ( $20.93 \times 10^{-6}$  ~  $148.59 \times 10^{-6}$ , 平均  $70.23 \times 10^{-6}$ ) 含量, 稀土元素配分曲线均呈平缓右倾, 轻稀土元素略相对富集, 富集大离子亲石元素(LILE)(如 Rb、Ba、Th、U、K), 亏损高场强元素(HFSE)(如 Ta、Nb、P、Ti)。这些特征类似于日本西南新生代 Setouchi 火山岩带赞岐岩。通过岩石成因分析, 认为该岩体很可能由俯冲洋壳和沉积物部分熔融产生的含水流体与地幔橄榄岩相互作用形成, 进而揭示其形成于岛弧环境。这表明红柳河-牛圈子-洗肠井古洋盆在晚奥陶世仍在向北俯冲, 哈萨克斯坦板块和塔里木板块最终的拼合时间可能在奥陶纪之后。

**关键词:** 高镁闪长岩; 锆石 U-Pb 定年; 岩石成因; 构造环境; 北山地区

中图分类号: P588.12<sup>+</sup>2; P597<sup>+</sup>.3

文献标识码: A

文章编号: 1000-6524(2018)04-0533-14

## Early Paleozoic subduction of the ocean in Beishan region: Zircon U-Pb geochronological and geochemical evidence from the high-Mg diorite in the Shibanjing area

ZHUAN Shao-peng, CHEN Chao, SHEN Zong-yi, PAN Zhi-long, ZHANG Yun-qiang, ZHAO Hua-ping,  
CHEN Hong-qiang, YANG Rui and XIU Di

(Institute of Regional Geological and Mineral Resource Survey of Hebei Province, Langfang 065000, China)

**Abstract:** The high-Mg diorites occur in the Shibanjing area of central Beishan orogenic belt and are dated at  $456 \pm 2$  Ma by the LA-ICP-MS zircon U-Pb method, which indicates that they were generated in the Late Ordovician. According to geochemical data, the high-Mg diorites belong to the sodic calc-alkaline series, the content of  $\text{SiO}_2$  is 51.94% ~ 55.30%. They are geochemically characterized by high  $\text{MgO}$  (4.12% ~ 6.19%, avg. 5.17%),  $\text{Mg}^{\#}$  (0.45 ~ 0.69, avg. 0.53),  $\text{Cr}$  ( $35.82 \times 10^{-6}$  ~  $985.50 \times 10^{-6}$ , avg.  $284.84 \times 10^{-6}$ ), and  $\text{Ni}$  ( $20.93 \times 10^{-6}$  ~  $148.59 \times 10^{-6}$ , avg.  $70.23 \times 10^{-6}$ ), and also exhibit nearly flat right-declined REE patterns with slight enrichment of LREE. The high-Mg diorites are strongly enriched in large-on-lithophile elements such as Rb, Ba, Th, U and K, and are characterized by depletion of high-field-strength elements such as Nb, Ta, P and Ti. These geochemical features are analogous to those of Cenozoic Setouchi volcanic belt in southwestern Japan. Petrogenesis

收稿日期: 2017-10-18; 接受日期: 2018-05-24

基金项目: 中国地质调查局地质调查项目(12120114064101)

作者简介: 专少鹏(1979-), 男, 副高级工程师, 主要从事区域地质矿产调查与研究工作; 通讯作者: 陈超(1984-), 男, 工程师, 主要从事区域地质矿产调查与研究工作, E-mail: chchgood@163.com。

analysis shows that the rock mass was probably formed by the interaction between the aqueous fluid produced by partial melting of subducted oceanic crust and sediments and the mantle peridotite, suggesting that it was formed in an island arc environment. It is thus concluded that the Hongliuhe-Niuquanzi-Xichangjing ancient ocean plate was presumably in the process of subduction during the late Ordovician, and the collision between Kazakhstan plate and the Tarim plate might have occurred after Ordovician.

**Key words:** high-Mg diorite; LA-ICP-MS zircon U-Pb dating; petrogenesis; tectonic setting; Beishan region

**Fund support:** Geological Survey Program of China Geological Survey(12120114064101)

高镁安山岩(high-Mg andesite, HMA)泛指MgO( $Mg^{\#}$ )含量较高的安山岩和部分英安岩类,以 $SiO_2 > 52\%$ ,富Mg( $MgO > 5\%$ ,  $Mg^{\#} > 0.45$ )、Cr、Ni为特征,演化了的高镁安山岩MgO含量可低到2%~3%( $Mg^{\#}$ 仍然较高),Cr、Ni等含量也相应降低,包括sanukite(赞岐岩)、高镁adakite(高镁埃达克岩)、boninite(玻安岩)和bajaite(巴哈岩)(Yogodzinski *et al.*, 1994; Tatsumi, 2001; 张旗等, 2005; 赵振华等, 2007)。该类岩石在日本Setouchi火山带、Bonin岛、墨西哥Baja地区和阿留申群岛等地均有出露(Rogers *et al.*, 1985; Calmus *et al.*, 2003)。由于该类岩石的成因研究对揭示地壳生长、洋壳或陆壳俯冲、地壳拆沉以及流体或熔体-地幔间的相互作用等方面具有非常重要的意义,因此受到地质学家的广泛关注(Saunders *et al.*, 1987; Kelemen, 1995; Yogodzinski *et al.*, 2001; Benoit *et al.*, 2002; Zhang *et al.*, 2003; Guivel *et al.*, 2006; Pallares *et al.*, 2007; Wang *et al.*, 2008; 邓晋福等, 2010; 唐功建等, 2010; 李小波等, 2015; 李玮等, 2016; 彭松柏等, 2016)。近年来,具有与高镁安山岩特征相似的高镁闪长岩被相继报道,成为一个新的研究热点(巫祥阳等, 2003; 付长亮等, 2010; 尹继元等, 2012)。

本文报道的高镁闪长岩出露于北山造山带中部地区石板井一带。北山造山带位于中亚造山带南缘,大地构造位置处于华北板块、塔里木板块和哈萨克斯坦板块交汇部位,是研究中亚造山带增生造山的关键地区之一(李锦铁等, 2009; Xiao *et al.*, 2010)。该地区大地构造背景十分复杂,岩浆活动非常活跃。目前,北山地区的构造单元划分、古洋盆开启、闭合时限等问题存在较多争议。左国朝等(2003)以芨芨台子-小黄山蛇绿混杂岩带为界,南北两侧分别划分为塔里木板块和哈萨克斯坦板块。刘雪亚等(1995)认为北山地区主体是哈萨克斯坦古板块的东延部分,骆驼峰、红石山和黑鹰山一线以北的中蒙边界地区在古生代属于西伯利亚古板块的南

缘,北山南麓的白山、红柳园、账房山一线以南的北山南缘及敦煌等地则属于塔里木古板块的东延部分。杨合群等(2008)、孟贵祥等(2009)、徐学义等(2008)认为北山地区涉及两个一级构造单元,以红柳河-牛圈子-洗肠井缝合带为界,北侧为哈萨克斯坦板块,南侧为塔里木板块。另外,部分学者通过对红柳河-井圈子-洗肠井蛇绿岩带的年代学方面进行研究,认为其形成于早古生代洋盆环境(杨合群等, 2010; 代文军, 2011; 武鹏等, 2012; 孙立新等, 2017),然而该洋盆的俯冲时限还缺乏精确的年代学证据。本文在北山中部石板井地区进行1:5万区域地质矿产调查的基础上,通过对新发现的高镁闪长岩进行岩石学、年代学和岩石地球化学等方面的研究,揭示其形成时代、岩石成因和构造背景,并探讨红柳河-牛圈子-洗肠井古洋盆的俯冲、闭合时限,从而为进一步研究北山地区大地构造演化提供依据。

## 1 地质背景

研究区位于北山造山带中部石板井地区,为红柳河-牛圈子-洗肠井洋盆向北俯冲所形成的岛弧带(何世平等, 2002),是认识北山地区构造演化的重要位置。区域上著名的红柳河-牛圈子-洗肠井蛇绿混杂岩带位于研究区南部,沿白云山-黄山-蒜井子一线通过(图1)。石板井-小黄山断裂带呈北西西向从区内中部穿过,表现为强烈的韧性变形特征。区内出露主要岩石地层有古元古代北山岩群、中-新元古代地层、早古生代地层和中生代地层。北山岩群分布于红柳河-牛圈子-洗肠井蛇绿混杂岩带以北地区,为一套高绿片岩-角闪岩相的古老变质结晶基底岩系,中新元古代地层出露于红柳河-牛圈子-洗肠井蛇绿混杂岩带以南,为一套滨浅海相碎屑岩、碳酸盐岩沉积建造,古生代地层为一套火山-碎屑沉积建造,中生代地层为一套陆相碎屑岩沉积建造。研究区侵入岩非常发育,岩石种类繁多,基性-酸性岩

石均有分布。基性、超基性岩类主要分布于石板井南的白云山一带,是构成红柳河-牛圈子-洗肠井蛇绿混杂岩带的重要岩石单元。中酸性岩类在研究区分布广泛,总体呈近东西向展布于红柳河-牛圈子-

洗肠井蛇绿混杂岩带以北,侵位时代以加里东中晚期和华力西早期为主,分布面积最大。本次工作在石板井西北部加里东中晚期中酸性侵入岩中新发现高镁闪长岩体,即本文研究对象。

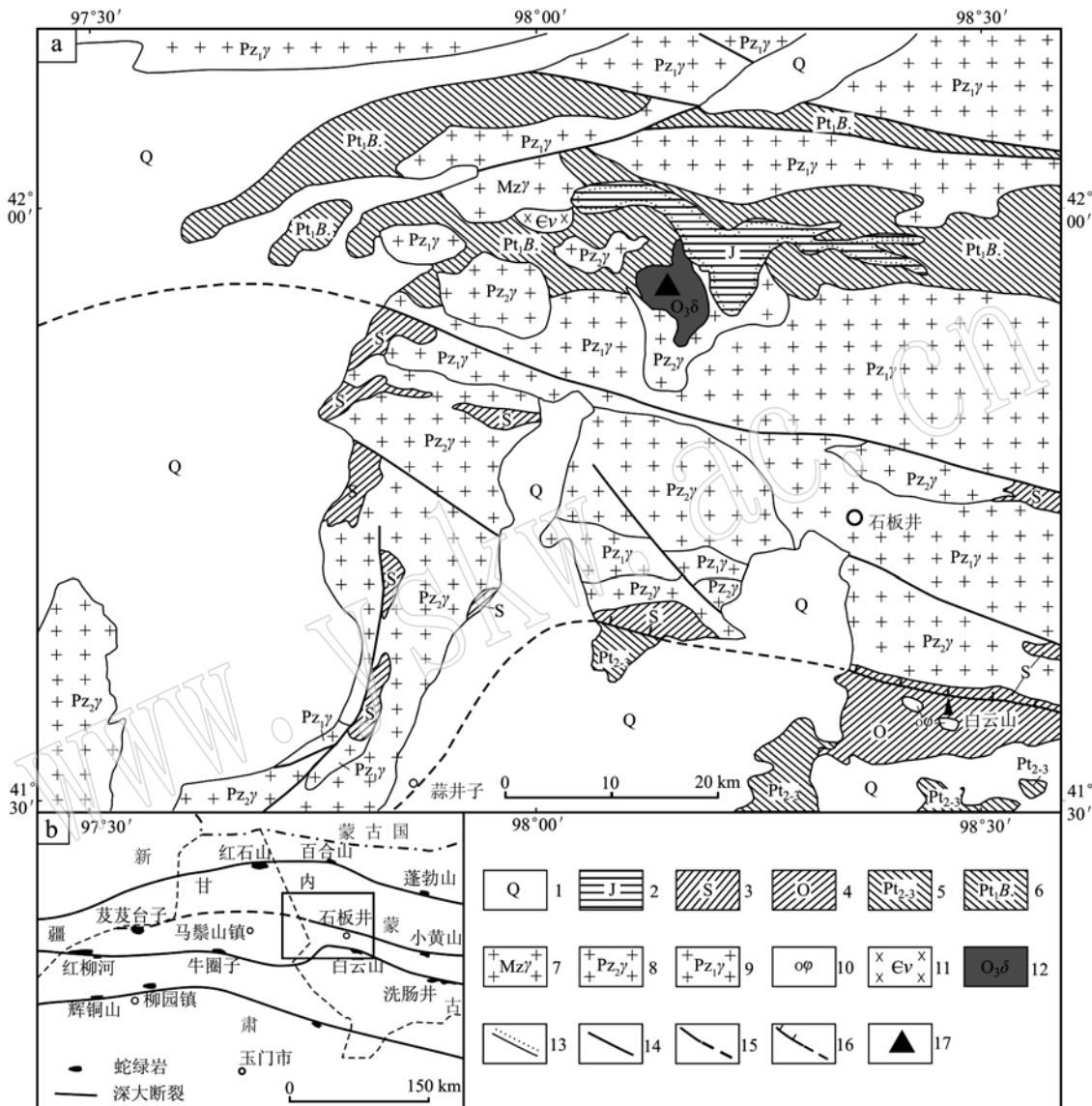


图1 北山石板井地区地质简图[a据陈超等(2016)<sup>①</sup>和潘志龙等(2015)<sup>②</sup>,b据杨合群等(2010)]

Fig. 1 Schematic geological map of the Shibanjing area, Beishan (a modified after Chen Chao et al., 2016<sup>①</sup> and Pan Zhilong et al., 2016<sup>②</sup>, b modified after Yang Hequn et al., 2010)

1—第四系; 2—侏罗纪地层; 3—志留纪地层; 4—奥陶纪地层; 5—中上元古界地层; 6—古元古界北山岩群; 7—中生代花岗岩体; 8—晚古生代花岗岩体; 9—早古生代花岗岩体; 10—蛇绿岩; 11—寒武纪辉长岩体; 12—中奥陶世闪长岩体; 13—不整合界线; 14—断层; 15—石板井-小黄山构造带; 16—牛圈子-洗肠井蛇绿混杂岩带; 17—采样位置

1—Quaternary; 2—Jurassic; 3—Silurian; 4—Ordovician; 5—Meso-Neoproterozoic; 6—Paleoproterozoic Beishan Group; 7—Mesozoic granite; 8—Late Paleozoic granite; 9—Early Paleozoic granite; 10—ophiolite mélange; 11—Cambrian bojite; 12—Middle Ordovician diorite; 13—unconformity; 14—fault; 15—Shibanjing-Xiaohuangshan structural belt; 16—Niujuanzhi-Xichangjing ophiolite belt; 17—sampling site

① 陈 超, 刘增校, 潘志龙, 等. 2016. 1:5万石板井等四幅区域地质矿产调查图.

② 潘志龙, 陈 超, 刘增校, 等. 2015. 1:5万基东等四幅区域地质矿产调查图.

## 2 岩体地质与岩相学特征

本次工作研究的闪长岩体位于红柳河-牛圈子-洗肠井蛇绿混杂岩带北侧的石板井西北部,出露面积约 $20\text{ km}^2$ ,呈岩珠状产出,侵入于古元古代北山岩群,接触带附近的闪长岩体内含有古元古代北山岩群二云母石英片岩捕掳体。该岩体被后期晚古生代花岗岩体侵入。闪长岩体岩性以闪长岩为主,辉长闪长岩少量,岩石组成矿物粒度不均匀,由岩体边部细粒结构向岩体中心渐变为中细粒结构。岩石普遍具有透入性变形,发育弱片麻状构造,片麻理走向近东西向,暗示曾遭受过近南北向挤压。本次工作在闪长岩体中采集1件锆石U-Pb同位素样品和5件岩石地球化学分析样品,采样位置见图1。样品均挑

选为新鲜无蚀变,且无脉体穿插的岩石。

闪长岩:岩石呈深灰色,中细粒半自形粒状结构,弱片麻状构造,组成矿物主要有斜长石(60%~65%)、石英(<5%)、角闪石(20%~25%)、黑云母(10%~15%)等,弱定向分布(图2a、2b)。斜长石主呈半自形板状,粒度一般为 $0.1\text{ mm} \times 0.2\text{ mm} \sim 0.5\text{ mm} \times 2.0\text{ mm}$ ,少量为 $0.5\text{ mm} \times 2.0\text{ mm} \sim 1.0\text{ mm} \times 2.5\text{ mm}$ ,环带构造较发育,部分可见聚片双晶,测得斜长石牌号 $\text{An} = 44$ ,属于中长石。石英呈它形粒状,粒度一般为 $0.2 \sim 1.0\text{ mm}$ ,填隙于斜长石粒间。角闪石呈半自形柱粒状,柱状角闪石粒度一般 $0.1\text{ mm} \times 0.2\text{ mm} \sim 0.5\text{ mm} \times 1.8\text{ mm}$ ,粒状角闪石粒度一般 $0.2 \sim 1.0\text{ mm}$ ,多色性较明显 $\text{Ng}' = \text{褐绿色}$ , $\text{Np}' = \text{浅黄绿色}$ 。黑云母呈鳞片状、叶片状,粒度一般 $0.5 \sim 1.6\text{ mm}$ ,少量穿插于角闪石粒内,交代角闪石。

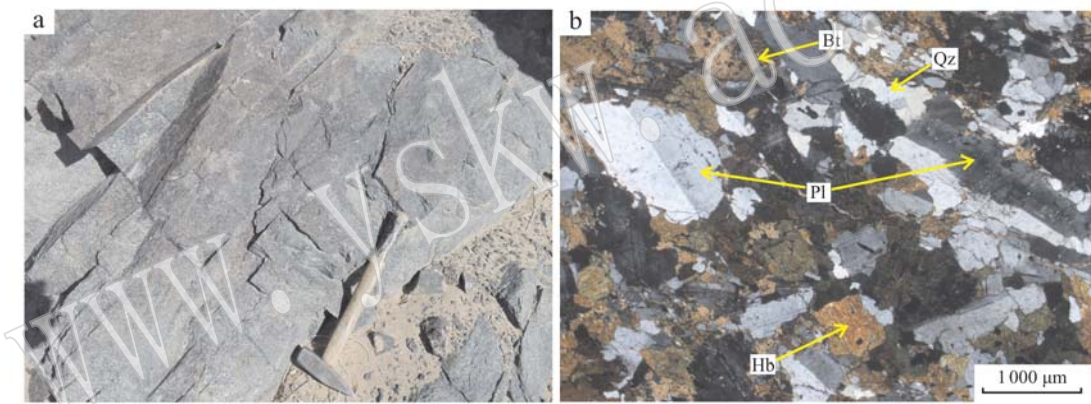


图2 石板井地区闪长岩野外特征及薄片显微特征(+)

Fig. 2 Field and microscopic photos of the diorite in the Shibanjing area(+)

Pl—斜长石; Hb—角闪石; Bt—黑云母; Q—石英

Pl—plagioclase; Hb—hornblende; Bt—biotite; Q—quartz

## 3 岩石地球化学特征

5件闪长岩地球化学样品主微量元素分析在河北地矿局廊坊实验室完成。主量元素采用XRF法和滴定法,XRF法采用荷兰帕纳科公司研制的Axios-X射线荧光光谱仪测定,分析精度优于2%;稀土和微量元素采用美国赛默飞世尔科技公司(ThermoFisherScientific)研制的XSeriesII型等离子体质谱仪(ICP-MS)测定,分析精度优于5%。主量元素、微量元素分析结果见表1。

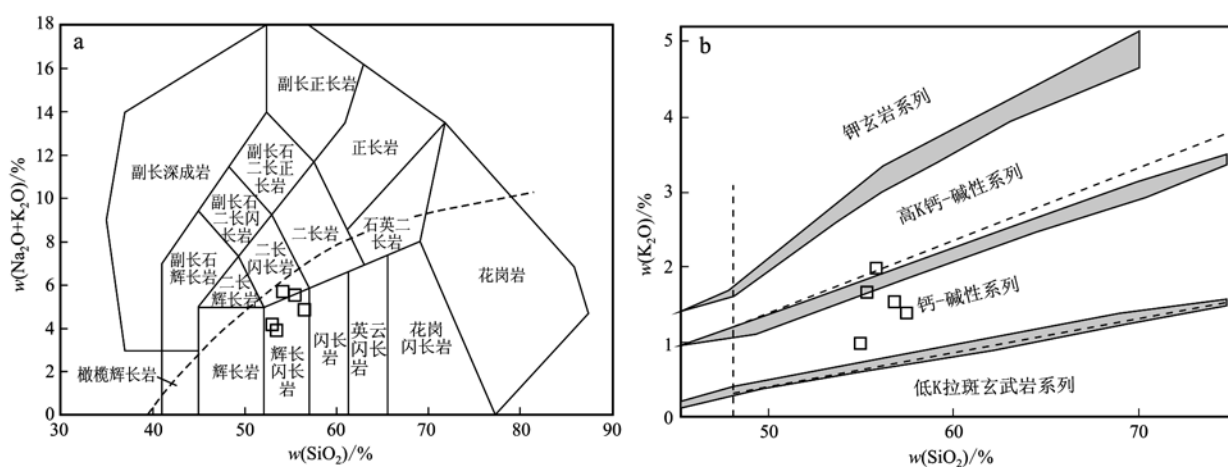
### 3.1 主量元素特征

闪长岩 $\text{SiO}_2$ 含量较低,介于51.94%~55.30%

之间;富 $\text{Al}_2\text{O}_3$ (15.50%~17.12%)、 $\text{FeO}^\text{T}$ (4.99%~9.86%)、 $\text{MgO}$ (4.12%~6.19%,平均5.17%>5%)和 $\text{CaO}$ (6.75%~8.80%); $\text{Mg}^\#$ 值较高,介于0.45~0.69之间,平均为0.53(>0.45);这些主量元素特征显示石板井闪长岩应属高镁闪长岩类。另外,部分主要特征氧化物与日本的Oto-Zan和East Setouchi高镁安山岩( $\text{MgO} = 2.58\% \sim 6.69\%$ , $\text{Al}_2\text{O}_3 = 14.21\% \sim 16.71\%$ , $\text{Mg}^\# = 0.58 \sim 0.72$ ,据Kawabata and Shuto, 2005和Tatsumi, 2006)相近。在TAS图解中,样品分布于Irvine线下方的亚碱性区域(图3a); $\text{K}_2\text{O}-\text{SiO}_2$ 图解中,样品全部落入钙碱性系列区域(图3b);A/NK-A/CNK图解中,样品属准铝质岩石(图4)。

表 1 石板井地区闪长岩主量元素( $w_B/\%$ )、微量元素和稀土元素( $w_B/10^{-6}$ )分析结果Table 1 Analytical results of major elements ( $w_B/\%$ ), trace elements and REE ( $w_B/10^{-6}$ ) concentrations of the diorite in Shibanjing area

| 样品编号                           | SBJ9   | SBJ10  | SBJ11  | SBJ12  | SBJ13  | 样品编号                 | SBJ9   | SBJ10  | SBJ11  | SBJ12  | SBJ13  |
|--------------------------------|--------|--------|--------|--------|--------|----------------------|--------|--------|--------|--------|--------|
| 岩性                             | 闪长岩    | 闪长岩    | 闪长岩    | 闪长岩    | 闪长岩    | 岩性                   | 闪长岩    | 闪长岩    | 闪长岩    | 闪长岩    | 闪长岩    |
| SiO <sub>2</sub>               | 55.30  | 52.93  | 52.14  | 51.94  | 54.39  | Ni                   | 148.59 | 20.93  | 31.42  | 41.52  | 108.69 |
| TiO <sub>2</sub>               | 1.09   | 1.92   | 1.13   | 1.08   | 0.74   | Cr                   | 985.50 | 35.82  | 137.28 | 167.11 | 98.52  |
| Al <sub>2</sub> O <sub>3</sub> | 17.04  | 16.37  | 15.50  | 16.39  | 17.12  | Ga                   | 21.93  | 27.14  | 16.80  | 18.58  | 14.76  |
| Fe <sub>2</sub> O <sub>3</sub> | 2.80   | 2.30   | 3.62   | 4.06   | 1.62   | Cs                   | 6.86   | 2.04   | 3.24   | 0.90   | 1.89   |
| FeO                            | 5.65   | 6.94   | 6.30   | 6.20   | 3.54   | Pb                   | 7.07   | 15.56  | 9.99   | 7.78   | 3.83   |
| MnO                            | 0.14   | 0.16   | 0.15   | 0.20   | 0.12   | Y                    | 37.81  | 45.02  | 17.94  | 22.97  | 13.84  |
| MgO                            | 4.13   | 4.12   | 6.18   | 5.26   | 6.19   | La                   | 33.01  | 34.90  | 16.40  | 11.67  | 17.34  |
| CaO                            | 6.75   | 7.09   | 8.46   | 8.65   | 8.80   | Ce                   | 77.71  | 80.80  | 36.10  | 23.37  | 33.25  |
| Na <sub>2</sub> O              | 3.41   | 3.62   | 2.19   | 3.13   | 3.92   | Pr                   | 10.46  | 10.40  | 4.82   | 3.19   | 4.62   |
| K <sub>2</sub> O               | 1.33   | 1.93   | 1.61   | 0.96   | 1.50   | Nd                   | 43.67  | 43.20  | 19.60  | 13.53  | 17.79  |
| P <sub>2</sub> O <sub>5</sub>  | 0.24   | 0.37   | 0.23   | 0.13   | 0.14   | Sm                   | 8.99   | 8.76   | 3.72   | 3.45   | 3.60   |
| LOI                            | 1.99   | 1.46   | 2.31   | 1.81   | 1.75   | Eu                   | 1.88   | 2.10   | 1.14   | 1.07   | 1.10   |
| Total                          | 99.86  | 99.21  | 99.81  | 99.82  | 99.82  | Gd                   | 7.22   | 7.51   | 3.21   | 2.69   | 2.82   |
| Mg <sup>#</sup>                | 0.47   | 0.45   | 0.54   | 0.49   | 0.69   | Tb                   | 1.30   | 1.47   | 0.59   | 0.61   | 0.51   |
| FeO <sup>T</sup>               | 8.17   | 9.00   | 9.56   | 9.86   | 4.99   | Dy                   | 7.20   | 8.06   | 3.18   | 4.39   | 2.90   |
| FeO <sup>T</sup> /MgO          | 1.98   | 2.19   | 1.55   | 1.88   | 0.81   | Ho                   | 1.39   | 1.58   | 0.60   | 0.88   | 0.53   |
| Rb                             | 92.40  | 86.37  | 59.08  | 15.87  | 26.23  | Er                   | 3.62   | 4.41   | 1.72   | 2.35   | 1.43   |
| Ba                             | 374.10 | 700.27 | 457.56 | 327.74 | 249.08 | Tm                   | 0.59   | 0.71   | 0.26   | 0.37   | 0.20   |
| Th                             | 6.83   | 3.31   | 5.15   | 4.18   | 4.50   | Yb                   | 3.36   | 4.57   | 1.81   | 2.48   | 1.31   |
| U                              | 1.79   | 1.56   | 1.34   | 0.73   | 1.39   | Lu                   | 0.45   | 0.62   | 0.27   | 0.39   | 0.24   |
| Ta                             | 1.79   | 1.40   | 0.64   | 0.54   | 0.67   | $\Sigma$ REE         | 200.85 | 209.09 | 93.42  | 70.44  | 87.62  |
| Nb                             | 13.58  | 25.29  | 9.08   | 6.92   | 7.74   | $\delta$ Eu          | 0.69   | 0.77   | 0.98   | 1.03   | 1.02   |
| Sr                             | 325.44 | 441.00 | 354.10 | 454.58 | 565.35 | (La/Yb) <sub>N</sub> | 7.04   | 5.48   | 6.50   | 3.37   | 9.46   |
| Zr                             | 237.78 | 287.66 | 129.62 | 90.66  | 136.58 | (La/Sm) <sub>N</sub> | 2.37   | 2.57   | 2.85   | 2.18   | 3.11   |
| Hf                             | 10.24  | 8.97   | 7.39   | 4.30   | 5.16   | (Gd/Yb) <sub>N</sub> | 1.78   | 1.36   | 1.47   | 0.90   | 1.78   |
| V                              | 153.60 | 184.18 | 212.49 | 246.81 | 79.98  | Sr/Y                 | 8.61   | 9.79   | 19.74  | 19.79  | 40.85  |

图 3 石板井地区闪长岩 TAS 图解(a, 据 Middlemost, 1994 和 Irvine, 1971) 和 K<sub>2</sub>O-SiO<sub>2</sub> 图解(b, 据 Rickwood, 1989)Fig. 3 TAS diagram (a, after Middlemost, 1994 and Irvine, 1971) and K<sub>2</sub>O-SiO<sub>2</sub> diagram (b, after Rickwood, 1989) of diorite in Shibanjing area

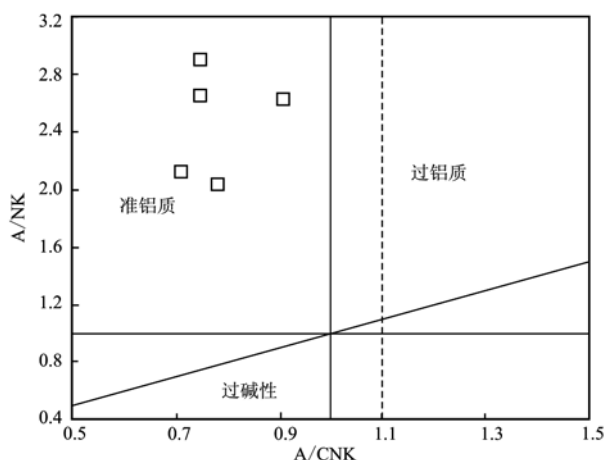


图4 石板井地区闪长岩A/NK - A/CNK图解(据 Peccerillo and Taylor, 1976)

Fig. 4 A/NK - A/CNK diagram of diorite in Shibanjing area  
(after Peccerillo and Taylor, 1976)

### 3.2 稀土元素和微量元素特征

石板井闪长岩稀土总量较高( $\Sigma \text{REE} = 70.44 \times 10^{-6} \sim 209.09 \times 10^{-6}$ )；轻、重稀土分馏不太明显 $[(\text{La/Yb})_N = 3.37 \sim 9.46]$ ；轻稀土分馏程度略高 $[\text{La/Sm}]_N = 2.18 \sim 3.11$ ，重稀土近乎平坦 $[(\text{Gd/Yb})_N = 0.90 \sim 1.78]$ ；具有弱负铕异常至无铕异常( $\delta \text{Eu} = 0.69 \sim 1.03$ ，平均0.90)。在REE球粒陨石标准化模式图(图5a)，闪长岩稀土配分曲线均呈平缓右倾，轻稀土略相对富集，重稀土分馏较弱，

与Setouchi火山岩带赞岐岩类稀土配分曲线形态基本一致(据Tatsumi, 1981, 1982, 2006; Shimoda *et al.*, 1998; Tatsumi and Hanyu, 2003)。微量元素具有较高的Cr( $35.82 \times 10^{-6} \sim 985.50 \times 10^{-6}$ ，平均 $284.84 \times 10^{-6}$ )、Ni( $20.93 \times 10^{-6} \sim 148.59 \times 10^{-6}$ ，平均 $70.23 \times 10^{-6}$ )含量，明显高于正常弧火山岩。原始地幔标准化微量元素蛛网图中(图5b)，表现为富集大离子亲石元素(LILE)Rb、Ba、Th、U、K等，亏损高场强元素(HFSE)Ta、Nb、P、Ti等，呈现出显著的“TNT”异常。

## 4 LA-ICP-MS 锆石 U-Pb 同位素定年

### 4.1 测试方法

锆石分选在河北省区域地质矿产调查研究所实验室利用标准重矿物分离技术分选完成。锆石的制靶和透射光、反射光、阴极发光照相均在北京锆年领航科技有限公司完成。通过反射光、透射光和阴极发光图像分析，选取具有明显震荡环带结构且无裂隙和包裹体的岩浆锆石进行测试。LA-ICP-MS 锆石 U-Pb 同位素测定在中国地质科学院地质研究所大陆构造与动力学实验室完成。激光剥蚀束斑直径为 $32 \mu\text{m}$ ，激光能量密度为 $10 \text{ J/cm}^2$ ，频率为8 Hz。数据分析前，采用国际上通用的锆石标样91500作为参考物质进行仪器的最佳化，选用GJ-1作为辅助

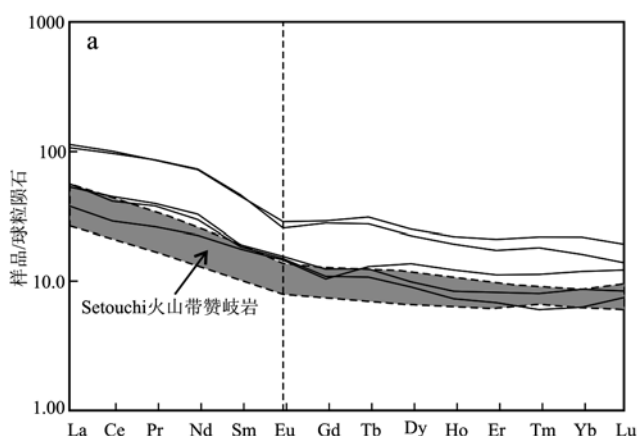


图5 石板井地区闪长岩球粒陨石标准化稀土元素配分图(a)和原始地幔标准化微量元素蛛网图(b)[ 标准化值据 Sun and McDonough (1989); Setouchi 火山岩带赞岐岩数据据 Tatsumi and Ishizaka (1981); Tatsumi and Ishizaka (1982); Shimoda *et al.* (1998); Tatsumi *et al.* (2003, 2006) ]

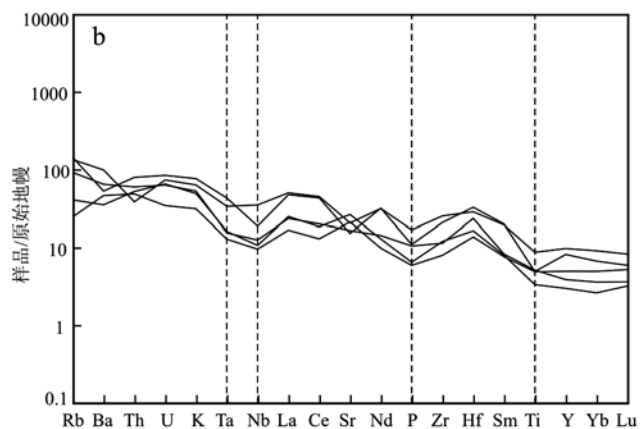


Fig. 5 Chondrite-normalized REE patterns (a) and primitive-mantle normalized spider diagram (b) of diorite in Shibanjing area  
(normalization values after Sun and McDonough, 1989; Setouchi volcanic belt sanukite values after Tatsumi *et al.*, 1981; Tatsumi and Ishizaka, 1982; Shimoda *et al.*, 1998; Tatsumi *et al.*, 2003, 2006)

标样对数据的准确性进行验证。数据处理采用 ICP-MSDataCal 程序 (Liu *et al.*, 2009), 年龄计算及谐和图绘制采用 Isoplot 程序 (Ludwig, 2003)。采用<sup>208</sup>Pb 校正法对普通 Pb 进行校正, 利用 NIST612 玻璃标样作为外标, 计算锆石样品的 Pb、U、Th 含量。

#### 4.2 测试结果

闪长岩样品 (TW01) 中的锆石颗粒无色透明, 半

自形-自形, 大小一般  $30 \mu\text{m} \times 50 \mu\text{m} \sim 80 \mu\text{m} \times 150 \mu\text{m}$ , 呈短柱状, 少部分呈长柱状, 长宽比约为 1.5:1 ~ 3:1。锆石内部结构具有较宽的结晶环带, 个别发育震荡环带 (图 6)。对晶形较好的 24 颗锆石共分析了 24 个测点, 测试数据及计算结果见表 2。锆石 U、Th 和 Pb 含量分别变化于  $139 \times 10^{-6} \sim 1 389 \times 10^{-6}$ 、 $41 \times 10^{-6} \sim 340 \times 10^{-6}$  和  $11 \times 10^{-6} \sim 59 \times 10^{-6}$ ,

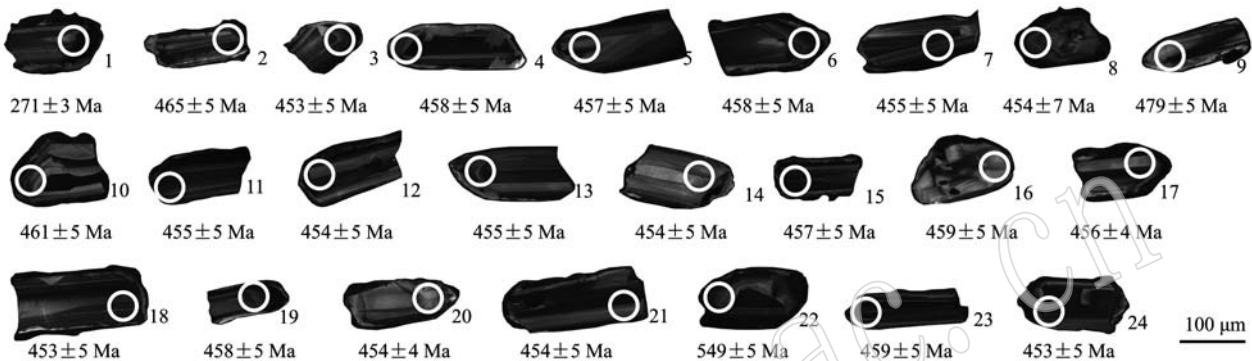


图 6 石板井地区闪长岩典型锆石 CL 图像及其年龄值

Fig. 6 Representative zircon CL images and ages of diorite in Shibanjing area

表 2 石板井地区闪长岩 LA-ICP-MS 锆石 U-Pb 同位素分析结果

Table 2 LA-ICP-MS zircon U-Th-Pb data for the diorite in Shibanjing area

| 测点 | $w_{\text{Pb}}/10^{-6}$ |       |     | 同位素比值                |                                  |           | 同位素年龄/Ma                         |           |                                   |           |                                  |           |                                  |           |                                   |           |
|----|-------------------------|-------|-----|----------------------|----------------------------------|-----------|----------------------------------|-----------|-----------------------------------|-----------|----------------------------------|-----------|----------------------------------|-----------|-----------------------------------|-----------|
|    | Pb                      | U     | Th  | $\text{Th}/\text{U}$ | $^{206}\text{Pb}/^{238}\text{U}$ | $1\sigma$ | $^{207}\text{Pb}/^{235}\text{U}$ | $1\sigma$ | $^{207}\text{Pb}/^{206}\text{Pb}$ | $1\sigma$ | $^{206}\text{Pb}/^{238}\text{U}$ | $1\sigma$ | $^{207}\text{Pb}/^{235}\text{U}$ | $1\sigma$ | $^{207}\text{Pb}/^{206}\text{Pb}$ | $1\sigma$ |
| 01 | 59                      | 1 389 | 213 | 0.15                 | 0.0429                           | 0.0005    | 0.4287                           | 0.0073    | 0.0725                            | 0.0010    | 270.7                            | 2.9       | 362.2                            | 6.2       | 999.6                             | 27.3      |
| 02 | 19                      | 218   | 240 | 1.10                 | 0.0749                           | 0.0007    | 0.5766                           | 0.0092    | 0.0559                            | 0.0008    | 465.4                            | 4.6       | 462.3                            | 7.3       | 447.0                             | 32.7      |
| 03 | 14                      | 172   | 140 | 0.82                 | 0.0728                           | 0.0007    | 0.5898                           | 0.0238    | 0.0587                            | 0.0023    | 453.2                            | 4.6       | 470.7                            | 19.0      | 557.3                             | 86.9      |
| 04 | 36                      | 437   | 340 | 0.78                 | 0.0736                           | 0.0008    | 0.5709                           | 0.0082    | 0.0563                            | 0.0007    | 457.8                            | 5.0       | 458.6                            | 6.6       | 462.7                             | 28.2      |
| 05 | 27                      | 317   | 297 | 0.94                 | 0.0735                           | 0.0007    | 0.5679                           | 0.0085    | 0.0560                            | 0.0008    | 457.2                            | 4.6       | 456.6                            | 6.9       | 453.7                             | 30.3      |
| 06 | 18                      | 231   | 102 | 0.44                 | 0.0737                           | 0.0007    | 0.5717                           | 0.0105    | 0.0563                            | 0.0010    | 458.2                            | 4.5       | 459.1                            | 8.5       | 463.3                             | 37.9      |
| 07 | 21                      | 255   | 178 | 0.70                 | 0.0732                           | 0.0008    | 0.5653                           | 0.0086    | 0.0560                            | 0.0008    | 455.2                            | 4.8       | 455.0                            | 6.9       | 453.8                             | 32.2      |
| 08 | 35                      | 473   | 109 | 0.23                 | 0.0729                           | 0.0012    | 0.5659                           | 0.0108    | 0.0563                            | 0.0007    | 453.6                            | 7.4       | 455.4                            | 8.7       | 464.5                             | 27.8      |
| 09 | 31                      | 328   | 309 | 0.94                 | 0.0772                           | 0.0007    | 0.6704                           | 0.0102    | 0.0630                            | 0.0009    | 479.2                            | 4.6       | 520.9                            | 7.9       | 708.1                             | 29.8      |
| 10 | 14                      | 185   | 66  | 0.36                 | 0.0741                           | 0.0007    | 0.5744                           | 0.0124    | 0.0562                            | 0.0012    | 460.7                            | 4.6       | 460.8                            | 9.9       | 461.4                             | 45.7      |
| 11 | 30                      | 345   | 272 | 0.79                 | 0.0731                           | 0.0008    | 0.5672                           | 0.0084    | 0.0563                            | 0.0008    | 454.6                            | 4.9       | 456.2                            | 6.7       | 464.0                             | 29.6      |
| 12 | 25                      | 331   | 115 | 0.35                 | 0.0730                           | 0.0007    | 0.5661                           | 0.0079    | 0.0563                            | 0.0007    | 454.1                            | 4.5       | 455.5                            | 6.3       | 462.5                             | 28.4      |
| 13 | 18                      | 236   | 106 | 0.45                 | 0.0732                           | 0.0008    | 0.5697                           | 0.0094    | 0.0564                            | 0.0008    | 455.5                            | 4.9       | 457.8                            | 7.6       | 469.5                             | 32.6      |
| 14 | 11                      | 148   | 56  | 0.37                 | 0.0730                           | 0.0008    | 0.5702                           | 0.0126    | 0.0567                            | 0.0012    | 454.1                            | 4.8       | 458.1                            | 10.1      | 478.5                             | 46.9      |
| 15 | 43                      | 574   | 198 | 0.34                 | 0.0734                           | 0.0007    | 0.5656                           | 0.0075    | 0.0558                            | 0.0007    | 456.9                            | 4.6       | 455.1                            | 6.1       | 446.3                             | 26.3      |
| 16 | 11                      | 139   | 61  | 0.44                 | 0.0738                           | 0.0008    | 0.5733                           | 0.0171    | 0.0563                            | 0.0016    | 459.2                            | 4.8       | 460.1                            | 13.7      | 464.9                             | 64.2      |
| 17 | 24                      | 284   | 219 | 0.77                 | 0.0733                           | 0.0007    | 0.5701                           | 0.0087    | 0.0564                            | 0.0008    | 456.0                            | 4.5       | 458.1                            | 7.0       | 468.5                             | 30.8      |
| 18 | 29                      | 346   | 275 | 0.80                 | 0.0728                           | 0.0008    | 0.5652                           | 0.0083    | 0.0563                            | 0.0008    | 452.9                            | 4.9       | 454.9                            | 6.7       | 465.0                             | 29.5      |
| 19 | 19                      | 261   | 63  | 0.24                 | 0.0736                           | 0.0008    | 0.5729                           | 0.0111    | 0.0564                            | 0.0011    | 457.9                            | 4.8       | 459.9                            | 8.9       | 469.9                             | 41.2      |
| 20 | 27                      | 380   | 71  | 0.19                 | 0.0730                           | 0.0007    | 0.5673                           | 0.0079    | 0.0563                            | 0.0007    | 454.3                            | 4.5       | 456.3                            | 6.4       | 466.0                             | 28.4      |
| 21 | 18                      | 225   | 159 | 0.70                 | 0.0729                           | 0.0007    | 0.5633                           | 0.0100    | 0.0560                            | 0.0009    | 453.8                            | 4.6       | 453.7                            | 8.0       | 453.4                             | 35.6      |
| 22 | 39                      | 369   | 107 | 0.29                 | 0.0888                           | 0.0009    | 1.5700                           | 0.0223    | 0.1282                            | 0.0017    | 548.7                            | 5.4       | 958.4                            | 13.6      | 2 073.0                           | 22.9      |
| 23 | 24                      | 300   | 197 | 0.66                 | 0.0738                           | 0.0008    | 0.5688                           | 0.0101    | 0.0559                            | 0.0009    | 458.8                            | 4.7       | 457.3                            | 8.1       | 449.6                             | 36.7      |
| 24 | 23                      | 329   | 41  | 0.13                 | 0.0727                           | 0.0007    | 0.5692                           | 0.0109    | 0.0568                            | 0.0010    | 452.5                            | 4.6       | 457.5                            | 8.8       | 482.3                             | 37.9      |

具有较高的 Th/U 值(0.13~1.10, 平均0.54), 显示了岩浆锆石的特点。1号测点 $^{206}\text{Pb}/^{238}\text{U}$ 年龄偏小(270.7 Ma), 10、22号测点 $^{206}\text{Pb}/^{238}\text{U}$ 年龄偏大(479.2 Ma、548.7 Ma), 并且明显偏离谐和曲线, 这可能与锆石的 Pb 丢失或加入有关, 亦或为捕获锆石; 其余21个测点的 $^{206}\text{Pb}/^{238}\text{U}$ 年龄比较接近, 介于465.4~452.5 Ma之间, 集中分布于谐和线上, 其加权平均年龄为 $456 \pm 2$  Ma( $N = 21$ , MSWD = 0.43) (图7), 代表了闪长岩的结晶年龄, 为晚奥陶世早期。

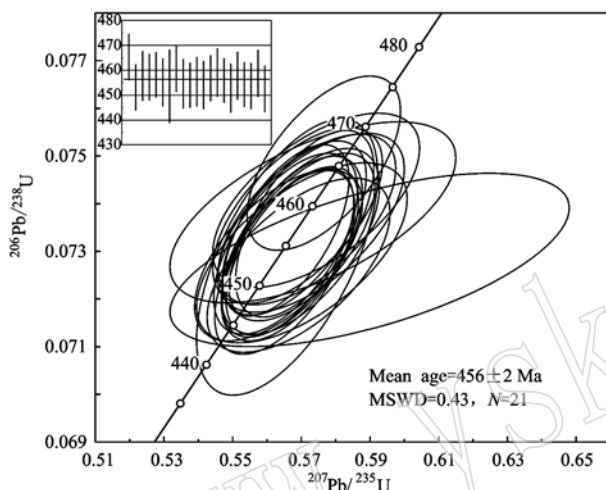


图7 石板井地区闪长岩 LA-ICP-MS 锆石 U-Pb 谐和图  
Fig. 7 LA-ICP-MS U-Pb concordia diagram of zircon in the diorite in the Shibanjing area

## 5 讨论

### 5.1 岩石成因

地球化学特征显示, 研究区内的石板井闪长岩体岩性属高镁闪长岩。目前研究表明, 高镁安山质岩浆的形成机制主要有: ①含水的地幔橄榄岩直接部分熔融的产物(Tatsumi, 1981; Wood and Turner, 2009); ②拆沉下地壳部分熔融的熔体与地幔橄榄岩相互反应的产物(Kelemen *et al.*, 1998; Smithies and Champion, 1999); ③富集地幔部分熔融的产物(Stern *et al.*, 1989; Stern and Hanson, 1991; Smithies and Champion, 2000); ④由消减板片部分熔融产生的熔体或流体与地幔楔反应形成(Yogodzinski *et al.*, 1995; Shimoda *et al.*, 1998; Rapp *et al.*, 1999; Kamei *et al.*, 2004)。实验岩石学结果显示, 含水地幔橄榄岩直接部分熔融产生的高镁安山质岩浆具较

高的 SiO<sub>2</sub>(54.35%~60.26%)和非常高的 Al<sub>2</sub>O<sub>3</sub>(17.24%~21.70%)以及较低的 FeO<sup>T</sup>(4.04%~4.65%)、CaO(8.53%~9.99%)含量(Hirose, 1997)。与此相比, 石板井高镁闪长岩的 SiO<sub>2</sub>(51.94%~55.30%)、Al<sub>2</sub>O<sub>3</sub>(15.50%~17.12%)、CaO(6.75%~8.80%)含量均较低, FeO<sup>T</sup>(4.99%~9.86%)含量较高, 暗示其不可能为含水地幔橄榄岩直接部分熔融的产物。前人研究表明, 加厚下地壳拆沉熔融产生的熔体与地幔反应产生的岩浆通常具有高 Sr、低 Y、Yb、高 Sr/Y、无水, 石榴子石为残留相等特征(Gao *et al.*, 2004), 如辽西四合屯早白垩世义县组高镁安山岩(Sr =  $620 \times 10^{-6}$ ~ $1\ 323 \times 10^{-6}$ , Y =  $12 \times 10^{-6}$ ~ $19 \times 10^{-6}$ , Yb =  $1.03 \times 10^{-6}$ ~ $1.88 \times 10^{-6}$ , Sr/Y = 32~88, 据王晓蕊等, 2005)和辽西彰武地区中生代高镁安山岩(Sr =  $671 \times 10^{-6}$ ~ $1\ 499 \times 10^{-6}$ , Y =  $13 \times 10^{-6}$ ~ $24 \times 10^{-6}$ , Yb =  $0.9 \times 10^{-6}$ ~ $2.0 \times 10^{-6}$ , Sr/Y = 34~155, 据黄华等, 2007)。本文样品具有偏低的 Sr( $325.44 \times 10^{-6}$ ~ $565.35 \times 10^{-6}$ , 平均  $428.09 \times 10^{-6}$ )和偏高的 Y( $13.84 \times 10^{-6}$ ~ $45.02 \times 10^{-6}$ , 平均  $27.52 \times 10^{-6}$ )、Yb( $1.31 \times 10^{-6}$ ~ $4.47 \times 10^{-6}$ , 平均  $2.71 \times 10^{-6}$ )含量, 以及较低的 Sr/Y(8.61~40.85, 平均 19.76)、(La/Yb)<sub>N</sub>(3.37~9.46, 平均 6.37), 显示源区无石榴子石残留相(尹继元等, 2012), 同时样品含有大量角闪石和黑云母等含水矿物, 指示岩浆具有较高的水逸度, 这些特征表明石板井高镁闪长岩亦非拆沉下地壳部分熔融的熔体与地幔橄榄岩相互反应的产物。

值得注意的是, 石板井高镁闪长岩地球化学特征与日本西南新生代 Setouchi 火山岩带赞岐岩, 以及吉林色洛河地区晚二叠世高镁安山岩(李承东等, 2007)、吉林珲春地区三叠纪高镁闪长岩(付长亮等, 2010)、新疆哈图早二叠世富镁闪长岩(尹继元等, 2012)的地球化学特征非常相近。在(La/Yb)<sub>N</sub>-Yb<sub>N</sub> 和 Sr/Y-Y 图解中, 所有样品均落入赞岐岩区域(图8), 暗示石板井高镁闪长岩的形成可能与赞岐岩具有相似的岩浆过程。目前, 对于赞岐岩的成因存在两种观点: 大部分学者认为其源区是由地幔橄榄岩与消减洋壳板片或沉积物部分熔融的富 Si 体质熔体或流体平衡反应形成(Shimoda *et al.*, 1998; Tatsumi and Hanyu, 2003; Tatsumi, 2006); 部分学者认为其源区由富集地幔直接熔融形成(Stern *et al.*, 1989; Stevenson *et al.*, 1999)。石板井高镁闪长岩与 Stern 等(1989)所定义的由富集地幔直接熔融形

成的赞岐岩( $MgO > 6\%$ 、 $Mg^{\#} > 0.6$ , Ni 和 Cr >  $100 \times 10^{-6}$ )相比,  $MgO$ (4.12% ~ 6.19%, 平均 5.17%)、 $Mg^{\#}$ (0.45 ~ 0.69, 平均为 0.53)、Ni( $20.93 \times 10^{-6}$  ~  $148.59 \times 10^{-6}$ , 平均  $70.23 \times 10^{-6}$ )较低, 表明其源区不同于由富集地幔直接熔融形成。样品相对富集大离子亲石元素(Rb、Ba、Th、U、K 等), 亏损高场强元素(Ta、Nb、P、Ti 等), 一般被解释为由于俯冲沉积岩物质对地幔楔的添加所致, 这种地球化学属性表明岩浆源区存在广泛的流体交代作用(李承东等, 2007)。Hart 等(1991)指出 Rb/Cs 是俯冲作用中代

表流体或熔体来源于沉积物的良好指示剂。在 Rb/Cs – K/Ba 和 Rb/Cs – K/Rb 图解(图 9), 石板井高镁闪长岩样品均靠近海相沉积岩区, 说明其交代地幔的物质主要来源于沉积物。另外, 岩石具有较高的 Ba/La 比值(11.33 ~ 28.08)和较低的 Th/Yb 比值(0.73 ~ 3.42), 说明消减洋壳板片产生的流体也参与了成岩过程(Woodhead *et al.*, 2001)。综上所述, 北山地区石板井高镁闪长岩可能由俯冲洋壳和沉积物部分熔融产生的含水流体与地幔橄榄岩相互作用形成。

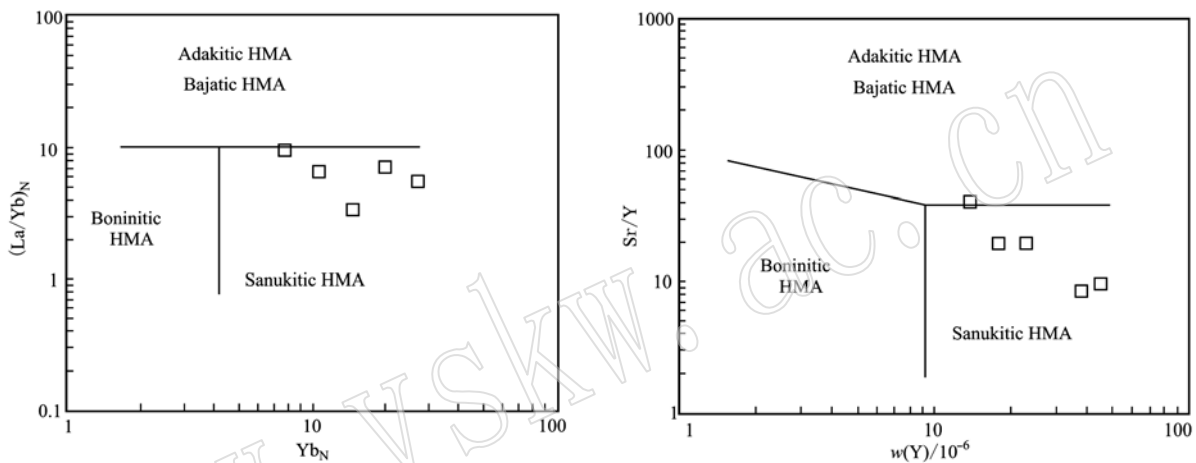


图 8 石板井地区高镁闪长岩分类图解(据 Kamei *et al.*, 2004)

Fig. 8 The discrimination diagram for high-Mg diorite in the Shibanjing area(after Kamei *et al.*, 2004)

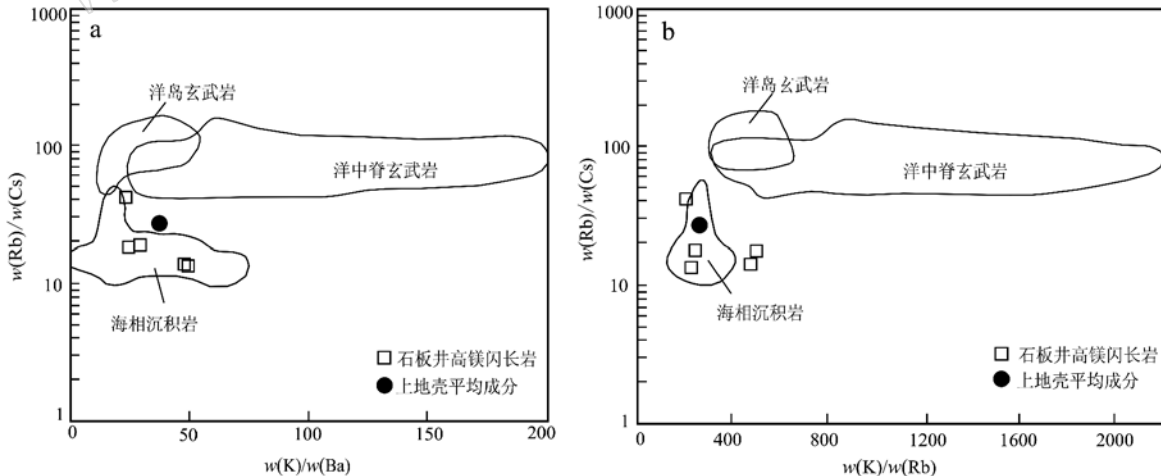


图 9 石板井地区高镁闪长岩 Rb/Cs – K/Ba 和 Rb/Cs – K/Rb 图解(据李承东等, 2007)

Fig. 9 Rb/Cs – K/Ba and Rb/Cs – K/Rb diagram for high-Mg diorites from Shibanjing area(after Li Chengdong *et al.*, 2007)

## 5.2 构造意义

通过 1:5 万区域地质矿产调查发现, 研究区内晚奥陶世侵入岩的岩石组合主要以高镁闪长岩-石

英闪长岩-英云闪长岩-花岗闪长岩为主, 具有典型俯冲带岩浆岩组合特征。地球化学研究结果显示, 石板井高镁闪长岩属准铝质钙碱性系列岩石, 富钠

( $\text{Na}_2\text{O}/\text{K}_2\text{O} = 1.35 \sim 3.27, > 1$ ), 富集 Rb、Ba、Th、U、K 等大离子亲石元素(LILE), 亏损 Ta、Nb、Ti 等高场强元素(HFSE), 具弱负铕异常至无铕异常( $\delta\text{Eu} = 0.69 \sim 1.03$ ), 显示出岛弧或者活动大陆边缘岩浆特点, 与形成俯冲带岛弧弧前构造环境高镁-镁质玄武安山岩-安山岩系[如阿留申岛弧岩浆岩中镁质安山岩、伊豆-小笠原-里亚纳(IBM)弧前高镁-镁质玄武安山岩-山岩即玻安岩系]的地球化学特征相似(Kay, 1978; Shirey and Hanson, 1984; Tatsumi, 1989; Defant and Drummond, 1990; Yodogaiński *et al.*, 1994; Shimoda *et al.*, 1998; Martin *et al.*, 2005; Hanyu *et al.*, 2006)。另外, 样品的稀土配分曲线形态与 Setouchi 火山岩带赞岐岩基本一致, 后者形成于菲律宾海板块年轻且热的岩石圈俯冲以及四国盆地的张开有关, 产于岛弧的弧前或弧后盆地环境(Tatsumi, 1982)。这些特征暗示石板井高镁闪长岩极可能亦形成与俯冲带有关的构造环境。岩石成因分析表明, 石板井高镁闪长岩可能由俯冲洋壳和沉积物部分熔融产生的含水流体与地幔橄榄岩相互作用形成, 然而具备这种形成条件的环境应为俯冲带。

北山造山带经历了古生代多期次、多阶段的板块裂解-俯冲-碰撞-拼合的复杂地质演化过程。北山地区古大陆自震旦纪有裂解前兆(左国朝等, 2003); 到寒武纪本区处于伸展构造体制(陈超等, 2017); 寒武纪至奥陶纪, 古大陆经过强烈的南北向扩张, 沿红柳河-牛圈子-洗肠井一带形成洋盆(何世平等, 2005); 奥陶纪末-志留纪, 红柳河-牛圈子-洗肠井洋盆发生自南向北的俯冲作用(杨合群等, 2012), 使洋盆北侧的哈萨克斯坦板块南缘成为活动陆缘, 并沿窑洞努如-公婆泉及白云山-斜山-东七一山一带形成岛弧带(龚全胜等, 2002)。石板井高镁闪长岩体产于红柳河-牛圈子-洗肠井洋盆北侧的白云山-斜山-东七一山早古生代岛弧带西段, 岩石地球化学特征指示其形成于岛弧环境, 与产出构造背景相吻合, 并且与南侧的红柳河-牛圈子-洗肠井古生代洋盆构成“沟-弧”体系。何世平等(2002)通过总结区域地质资料认为北山地区早古生代末结束了板块构造格局, 红柳河-牛圈子-洗肠井大洋封闭, 哈萨克斯坦板块和塔里木板块发生拼贴。张元元等(2008)在红柳河一带获得侵入蛇绿岩中未变形变质的花岗岩的年龄为  $404.8 \pm 5.2$  Ma, 据此认为红柳河-牛圈子-洗肠井洋盆在早泥盆世之前于红柳河地区闭合。综上所述, 本文认为晚奥陶世早期, 在石板井

地区红柳河-牛圈子-洗肠井洋盆向北侧哈萨克斯坦板块俯冲, 并且俯冲过程可能持续至早古生代末期。

## 6 结论

(1) 应用 LA-ICP-MS 方法测得北山地区石板井闪长岩体的锆石  $^{206}\text{Pb}/^{238}\text{U}$  年龄为  $456 \pm 2$  Ma ( $N = 21$ , MSWD = 0.43), 该年龄可以代表其形成年龄, 为晚奥陶世早期。

(2) 石板井闪长岩体岩性属钠质钙碱性系列的高镁闪长岩, 地球化学特征与赞岐岩相似, 可能由俯冲洋壳和沉积物部分熔融产生的含水流体与地幔橄榄岩相互作用形成。

(3) 石板井高镁闪长岩形成于岛弧环境, 表明本区存在早古生代消减带, 南侧红柳河-牛圈子-洗肠井古洋盆在晚奥陶世早期向北侧哈萨克斯坦板块俯冲, 俯冲可能持续至早古生代末期。

**致谢** 中国地质调查局天津地质调查中心王惠初、辛后田高级工程师为本项目的立项, 给予了大力支持; 在野外工作中得到河北省区域地质矿产调查研究所张计东、魏文通高级工程师的指导; LA-ICP-MS 锆石 U-Pb 同位素分析得到了中国地质科学院大陆构造与动力学实验室吴才来研究员的帮助; 评审专家对文章提出了诸多宝贵意见, 在此一并表示衷心感谢!

## References

- Benoit M, Aguillon-Robles A, Calmus T, *et al.* 2002. Geochemical diversity of Late Miocene volcanism in southern Baja California, Mexico: Implication of mantle and crustal sources during the opening of an asthenospheric window[J]. Journal of Geology, 110(6): 627~648.
- Calmus T, Aguillon-Robles A, Maury R C, *et al.* 2003. Spatial and temporal evolution of basalts and magnesian andesites (“bajaitas”) from Baja California, Mexico: The role of slab melts[J]. Lithos, 66(1~2): 77~105.
- Chen Chao, Xiu Di, Pan Zhilong, *et al.* 2017. Early paleozoic crustal extensional tectonic regime in the central part of Beishan orogenic belt: new evidence from geochronology and Geochemistry of Gabbro in Shibanjing [J]. Acta Geologica Sinica, 91(8): 1661~1673(in Chinese).
- Dai Wenjun. 2011. The formation background and tectonic significance of

- the ophiolite mélange in the Niuquanzi area, Beishan, Gansu province[J]. *Jmineral Petrol*, 31(4): 44 ~ 51(in Chinese).
- Defant M J and Drummond M S. 1990. Derivation of some modern arc magmas by melting of young subducted Lithosphere[J]. *Nature*, 347(6 291): 662 ~ 665.
- Deng Jinfu, Liu Cui, Feng Yanfang, et al. 2010. High magnesian andesitic/dioritic rocks (HMA) and magnesian andesitic/dioritic rocks (MA): two igneous rock types related to oceanic subduction[J]. *Geology in China*, 37(4): 1 112 ~ 1 118(in Chinese).
- Fu Changliang, Sun Deyou, Zhang Xingzhou, et al. 2010. Discovery and geological significance of the Triassic high-Mg diorites in Hunchu area, Jilin Province[J]. *Acta Petrologica Sinica*, 26 (4): 1 089 ~ 1 102(in Chinese).
- Gao S, Rudnick R L, Yuan H L, et al. 2004. Recycling lower continental crust in the North China craton[J]. *Nature*, 432(7 019): 892 ~ 897.
- Gong Quansheng, Liu Mingqiang, Li Hailin, et al. 2002. The type and basic characteristics of Beishan orogenic belt, Gansu[J]. *Northwestern Geology*, 35(3): 28 ~ 34(in Chinese).
- Guivel C, Morata D, Pelleter E, et al. 2006. Miocene to Late Quaternary Patagonian basalts( $46^{\circ}\sim 47^{\circ}$ S): Geochronometric and geochemical evidence for slab tearing due to active spreading ridge subduction [J]. *Journal of Volcanology and Geothermal Research*, 149(3 ~ 4): 346 ~ 370.
- Hanyu T, Tatsumi Y, Nakai S, et al. 2006. Contribution of slab melting and slab dehydration to magmatism in the NE Japanese arc for the last 25 Myr: Constraints from geochemistry[J]. *Geochemistry Geophysics Geosystems*, 7(8): 1 ~ 29.
- Hart and Reid. 1991. Rb/Cs fractionation: a Link between granulite metamorphism and the S-process[J]. *Geochim. Cosmochim. Acta*, 55: 2 379 ~ 2 383.
- He Shiping, Ren Bingchen, Yao Wenguang, et al. 2002. The division of tectonic units of Beishan area, Gansu-Inner Mongolia[J]. *Northwestern Geology*, 35(4): 30 ~ 40(in Chinese).
- He Shiping, Zhou Huiwu, Ren Bingchen, et al. 2005. Crustal evolution of Palaeozoic in Beishan area, Gansu and Inner Mongolia, China[J]. *Northwestern Geology*, 38(3): 6 ~ 15(in Chinese).
- Hirose K. 1997. Melting experiments on Iherzolite KLB-1 under hydrous conditions and generation of high-magnesian andesitic melts[J]. *Geology*, 25 (1): 42 ~ 44.
- Huang Hua, Gao Shan, Hu Zhaochu, et al. 2007. Geochemistry of the high-Mg andesites at Zhangwu, western Liaoning: Implication for delamination of newly formed lower crust[J]. *Science in China ( Series D )*, 50 (12): 1 773 ~ 1 786(in Chinese).
- Irvine T N and Baragar W R. 1971. A guide to the chemical classification of the common volcanic rocks[J]. *Canad. J. Earth Sci.*, 8: 523 ~ 548.
- Kamei A, Owada M, Nagao T, et al. 2004. high-Mg diorites derived from sanukitic HMA magmas, Kyushu Island, southwest Japan arc: Evidence from clinopyroxene and whole rock compositions[J]. *Lithos*, 75(3 ~ 4): 359 ~ 371.
- Kawabata H and Shuto K. 2005. Magma mixing recorded in intermediate rocks associated with high-Mg andesites from the Setouchi volcanic belt, Japan: implications for Archean TTG formation[J]. *Journal of Volcanology and Geothermal Research*, 140: 241 ~ 271.
- Kay R W. 1978. Aleutian magnesian andesites: melts from subducted Pacific ocean crust[J]. *Journal of Volcanology and Geothermal Resear*, 4(1 ~ 2): 117 ~ 132.
- Kelemen P B. 1995. Genesis of high Mg-number andesites and the continental-crust[J]. *Contributions to Mineralogy and Petrology*, 120 (1): 1 ~ 19.
- Kelemen P B, Hart S R and Bernstein S. 1998. Silica enrichment in the continental upper mantle via melt/rock reaction[J]. *Earth and Planetary Science Letters*, 164 (1 ~ 2): 387 ~ 406.
- Li Chengdong, Zhang Fuqin, Miao Laicheng, et al. 2007. Zircon SHRIMP geochronology and geochemistry of Late Permian high-Mg andesites in Seluohu area, Jilin province, China[J]. *Acta Petrologica Sinica*, 23(4): 767 ~ 776(in Chinese).
- Li Jinyi, Zhang Jin, Yang Tiannan, et al. 2009. Crustal tectonic division and evolution of the Southern part of the North Asian orogenic region and its adjacent areas[J]. *Journal of Jilin University(Earth Science Edition)*, 39(4): 584 ~ 605(in Chinese).
- Li Wei, Chen Junlu, Dong Yunpeng, et al. 2016. Early Paleozoic subduction of the Paleo-Asian Ocean: Zircon U-Pb geochronological and geochemical evidence from the Kalatag high-Mg andesites, East Tianshan[J]. *Acta Petrologica Sinica*, 32(2): 505 ~ 521(in Chinese).
- Li Xiaobo, Wang Baodi, Liu Han, et al. 2015. The Late Jurassic high-Mg andesites in the Daru Tso area, Tibet: Evidence for the subduction of the Bangong Co-Nujiang River oceanic lithosphere[J]. *Geological Bulletin of China*, 34(2/3): 251 ~ 261(in Chinese).
- Liu Xueya and Wang Quan. 1995. Tectonics of orogenic belts in Beishan Mts., Western China[J]. *Dixue Yanjiu*, 28(1): 37 ~ 48(in Chinese).
- Liu Y S, Gao S, Hu Z C, et al. 2009. Continental and oceanic crust recycling-induced melt-peridotite interactions in the Trans North China

- Orogen: U-Pb dating, Hf isotopes and trace elements in zircons from mantle xenoliths[J]. *Journal of Petrology*, 51: 537 ~ 571.
- Ludwig K R. 2003. Isoplot/EX version 2.49. A Geochronological Toolkit for Microsoft Excel[M]. Berkeley: Berkeley Geochronology Center Special Publication No. 1a, 1 ~ 56.
- Martin H, Smithies R H, Rapp R, et al. 2005. An overview of adakite, tonalite-trondhjemite-tranodiorite( TTG ), and sanukitoid: Relationships and same implications for crustal evolution[J]. *Lithos*, 79( 1 ~ 2 ): 1 ~ 24.
- Meng Guixiang, Lü Qingtian, Yan Jiayong, et al. 2009. Iron metallogenetic characteristics and prospecting potential of Beishan area, Inner Mongolia[J]. *Mineral Deposits*, 28( 6 ): 815 ~ 829( in Chinese ).
- Middlemost E A K. 1994. Naming materials in the magma/igneous rock system[J]. *Earth Science Research*, 37: 215 ~ 224.
- Pallares C, Maury R C, Bellon H, et al. 2007. Slab-tearing following ridge-trench collision: Evidence from Miocene volcanism in Baja California, Mexico[J]. *Journal of Volcanology and Geothermal Research*, 161( 1 ~ 2 ): 95 ~ 117.
- Peccerillo R and Taylor S R. 1976. Geochemistry of Eocene calc-alkaline volcanic rocks from the Kastamonu area, northern Turkey[J]. *Contrib. Mineral. Petrol.*, 58: 63 ~ 81.
- Peng Songbai, Liu Songfeng, Lin Musen, et al. 2016. Early Paleozoic subduction in cathaysia( II ): new evidence from the Dashuang high magnesian-magnesian andesite[J]. *Earth Science*, 41( 6 ): 931 ~ 947( in Chinese ).
- Rapp R P, Shimizu N, Norman M D, et al. 1999. Reaction between slab-derived melts and peridotite in the mantle wedge: Experimental constraints at 3.8 GPa[J]. *Chemical Geology*, 160( 4 ): 335 ~ 356.
- Rickwood P C. 1989. Boundary lines within petrologic diagrams which use oxides of major and minor elements[J]. *Lithos*, 22( 4 ): 247 ~ 263.
- Rogers G, Saunders A D, Terrell D J, et al. 1985. Geochemistry of Holocene volcanic rocks associated with ridge subduction in Baja California, Mexico[J]. *Nature*, 315( 6 018 ): 389 ~ 392.
- Saunders A D, Rogers G, Marriner G F, et al. 1987. Geochemistry of Cenozoic volcanic rocks, Baja California, Mexico: Implications for the petrogenesis of post-subduction magmas[J]. *Journal of Volcanology and Geothermal Research*, 32( 1 ~ 3 ): 223 ~ 245.
- Shimoda G, Tatsumi Y, Nohda S, et al. 1998. Setouchi high-Mg andesites revisited: Geochemical evidence for melting of subducting sediments[J]. *Earth and Planetary Science Letters*, 160( 3 ~ 4 ): 479 ~ 492.
- Shirey S B and Hanson G N. 1984. Mantle-derived archaean monozodiorites and trachyandesites[J]. *Nature*, 310: 222 ~ 224.
- Smithies R H and Champion D C. 1999. Late Archaean felsic alkaline igneous rocks in the Eastern Goldfields, Yilgarn Craton, Western Australia: A result of lower crustal delamination[J]. *Journal of the Geological Society*, 156: 561 ~ 576.
- Smithies R H and Champion D C. 2000. The Archaean high-Mg diorite suite: Links to tonalite-trondhjemite-granodiorite magmatism and implications for Early Archean crustal growth[J]. *Journal of Petrology*, 41( 12 ): 1 653 ~ 1 671.
- Stern R A and Hanson G N. 1991. Archean high-Mg granodiorite: A derivative of light rare earth element-enriched monzodiorite of mantle origin[J]. *Journal of Petrology*, 32( 1 ): 201 ~ 238.
- Stern R A, Hanson G N and Shirey S B. 1989. Petrogenesis of mantle-derived, LILE-enriched Archean monzodiorites and trachyandesites (sanukitoids) in southwestern Superior Province[J]. *Canadian Journal of Earth Sciences*, 26( 9 ): 1 688 ~ 1 712.
- Stevenson R, Herry P and Gariepy C. 1999. Assimilation-fractional crystallization origin of Archean sanukitoid suites: Western Superior Province, Canada[J]. *Precambrian Res.*, 96: 83 ~ 89.
- Sun Lixin, Zhang Jiahui, Ren Bangfang, et al. 2017. Geochemical characteristics and U-Pb age of Baiyunshan ophiolite melange in the Beishan orogenic belt and their geological implications[J]. *Acta Petrologica et Mineralogica*, 36( 2 ): 131 ~ 147( in Chinese ).
- Sun S S and McDonough W F. 1989. Chemical and isotopic systematics of oceanic basalts: Implications for mantle composition and processes [J]. London: Geological Society Special Publication, 42: 313 ~ 345.
- Tang Gongjian and Wang Qiang. 2010. High-Mg andesites and their geodynamic implications[J]. *Acta Petrologica Sinica*, 26( 8 ): 2 495 ~ 2 512( in Chinese ).
- Tatsumi Y. 1981. Melting experiments on a high-magnesian andesite[J]. *Earth and Planetary Science Letters*, 54 ( 2 ): 357 ~ 365.
- Tatsumi Y. 1982. Origin of high-magnesian andesites in the Setouchi volcanic belt, southwest, Japan, II. Melting phase relations at high pressures[J]. *Earth and Planetary Science Letters*, 60( 2 ): 305 ~ 317.
- Tatsumi Y. 1989. Migration of fluid phases and genesis of basalt magmas in subduction zones[J]. *Journal of Geophysical Research: Solid Earth*, 94( B4 ): 1 697 ~ 1 707.
- Tatsumi Y. 2001. Geochemical modeling of partial melting of subducting sediments and subsequent melt-mantle interaction: Generation of high-Mg andesites in the Setouchi volcanic belt, southwest, Japan [J]. *Geology*, 29( 4 ): 323 ~ 326.
- Tatsumi Y. 2006. High-Mg andesites in the Setouchi volcanic belt, south-

- western, Japan: Analogy to Archean magmatism and continental crust formation[J]. *Annual Review of Earth and Planetary Sciences*, 34: 467 ~ 499.
- Tatsumi Y and Hanyu T. 2003. Geochemical modeling of dehydration and partial melting of subducting lithosphere: Toward a comprehensive understanding of high-Mg andesite formation in the Setouchi volcanic belt, SW Japan [J]. *Geochemistry, Geophysics, Geosystems*, 4 (9): 1 ~ 19.
- Tatsumi Y and Lshizaka K. 1981. Existence of andesitic primary magma: An example from southwest Japan[J]. *Earth and Planetary Science Letters*, 53(1): 124 ~ 130.
- Tatsumi Y and Lshizaka K. 1982. Origin of high-magnesian andesites in the Setouchi volcanic belt, southwest, Japan I: Petrographical and chemical characteristics[J]. *Earth Planet Sci. Lett.*, 60(2): 293 ~ 304.
- Tatsumi Y, Shukuno H, Sato K, et al. 2003. The petrology and geochemistry of high-magnesium andesites at the western tip of the Setouchi Volcanic Belt, SW, Japan[J]. *Journal of Petrology*, 44(9): 1 561 ~ 1 578.
- Tatsumi Y, Suzuki T, Kawabata H, et al. 2006. The petrology and geochemistry of Oto-Zan Composite lava flow on Shodo-Shima Island, SW Japan: Remelting of a solidified high-Mg andesite magma[J]. *Journal of Petrology*, 47 (3): 595 ~ 629.
- Wang Q, Wyman D, Xu J, et al. 2008. Triassic Nb-enriched basalts, magnesian andesites, and adakites of the Qiangtang terrane (Central Tibet): Evidence for metasomatism by slab-derived melts in the mantle wedge[J]. *Contributions to Mineralogy and Petrology*, 155(4): 473 ~ 490.
- Wang Xiaorui, Gao Shan, Liu Xiaoming, et al. 2005. Geochemistry of the high-magnesium andesite of Early Cretaceous Yixian Formation in Sihertun, western Liaoning Province: Constraint on the delamination of lower crust and indication to the variation of Sr/Y ratio[J]. *Science in China (Series D)*, 35(8): 700 ~ 709 (in Chinese).
- Wood B J and Turner S P. 2009. Origin of primitive high-Mg andesite: Constraints from natural examples and experiments[J]. *Earth and Planetary Science Letters*, 283 (1 ~ 4): 59 ~ 66.
- Woodhead J D, Hergt J M, Davidson, et al. 2001. Hafnium isotope evidence for “conservative” element mobility during subduction zone processes[J]. *Earth and Planetary Science Letters*, 192: 331 ~ 346.
- Wu Peng, Wang Guoqiang, Li Xiangmin, et al. 2012. The age of Niujuanzi ophiolite in Beishan area of Gansu Province and its geological significance[J]. *Geological Bulletin of China*, 31(12): 2 032 ~ 2 037 (in Chinese).
- Wu Xiangyang, Xu Yigang, Ma Jinlong, et al. 2003. Geochemistry and petrogenesis of the Mesozoic high-Mg diorites from western Shandong [J]. *Geotectonica et Metallogenesis*, 27(3): 228 ~ 236 (in Chinese).
- Xiao W J, Mao Q G, Windley B F, et al. 2010. Paleozoic multiple accretionary and collisional processes of the Beishan orogenic collage[J]. *American Journal of Science*, 310(10): 1 553 ~ 1 594.
- Xu Xueyi, He Shiping, Wang Hongliang, et al. 2008. Outline of the Geology of NW China-Qinling, Qilian and Tian Shan Areas[M]. Beijing: Science Press, 1 ~ 347 (in Chinese) .
- Yang Hequn, Li Ying, Li Wenming, et al. 2008. General Discussion on Metallogenetic Tectonic Setting of Beishan Mountain, Northwestern China[J]. *Northwestern Geology*, 41(1): 22 ~ 28 (in Chinese).
- Yang Hequn, Li Ying, Zhao Guobin, et al. 2010. Character and structural attribute of the Beishan ophiolite[J]. *Northwestern Geology*, 43 (1): 26 ~ 36 (in Chinese).
- Yang Hequn, Zhao Guobin, Li Ying, et al. 2012. The relationship between Paleozoic tectonic setting and mineralization in Xinjiang-Gansu-Inner Mongolia juncture area[J]. *Geological Bulletin of China*, 31(2 ~ 3): 413 ~ 421 (in Chinese).
- Yin Jiyuan, Yuan Chao, Sun Min, et al. 2012. Age, geochemical features and possible petrogenesis mechanism of Early Permian magnesian diorite in Hatu, Xinjiang[J]. *Acta Petrologica Sinica*, 28 (7): 2 171 ~ 2 182 (in Chinese).
- Yogodzinski G M, Volynets O N, Koloskov A V, et al. 1994. Magnesian andesites and the subduction component in a strongly calc-alkaline series at Piip Volcano, Far Western Aleutians[J]. *Journal of Petrology*, 35(1): 163 ~ 204.
- Yogodzinski G M, Kay R W, Volynets O N, et al. 1995. Magnesian andesite in the western Aleutian Komandorsky Region: Implications for slab melting and processes in the mantle wedge[J]. *Geological Society of America Bulletin*, 107(5): 505 ~ 519.
- Yogodzinski G M, Lees J M, Churikova T G, et al. 2001. Geochemical evidence for the melting of subducting oceanic lithosphere at plate edges[J]. *Nature*, 409(6 819): 500 ~ 504.
- Zhang H F, Sun M, Zhou X H, et al. 2003. Secular evolution of the lithosphere beneath the eastern North China Craton: Evidence from Mesozoic basalts and high-Mg andesites[J]. *Geochimica et Cosmochimica Acta*, 67(22): 4 373 ~ 4 387.
- Zhang Qi, Qian Qing, Zhai Mingguo, et al. 2005. Geochemistry, petrogenesis and geodynamic implications of sanukite[J]. *Acta Petrologica et Mineralogica*, 24 (2): 117 ~ 125 (in Chinese).
- Zhang Yuanyuan and Guo Shaojie. 2008. Accurate constraint on formation

- and emplacement age of Hongliuhe ophiolite, boundary region between Xinjiang and Gansu Provinces and its tectonic implications [J]. *Acta Petrologica Sinica*, 24(4): 803~809 (in Chinese).
- Zhao Zhenhua, Wang Qiang, Xiong Xiaolin, et al. 2007. Magnesian igneous rocks in northern Xinjiang [J]. *Acta Petrologica Sinica*, 23(7): 1 696~1 707 (in Chinese).
- Zuo Guochao, Liu Yike and Liu Chunyan. 2003. Framework and evolution of the tectonic structure in Beishan area across Gansu province, Xinjiang autonomous region and inner Mongolia autonomous region [J]. *Acta Geologica Gansu*, 12(1): 1~15 (in Chinese).
- ### 附中文参考文献
- 陈超,修迪,潘志龙,等. 2017. 北山造山带中部早古生代伸展构造体制:来自石板井辉长岩的年代学及地球化学证据[J]. 地质学报, 91(8): 1 661~1 673.
- 代文军. 2011. 甘肃北山牛圈子蛇绿混杂岩的形成环境及构造意义[J]. 矿物岩石, 31(4): 44~51.
- 邓晋福,刘翠,冯艳芳,等. 2010. 高镁安山岩/闪长岩类(HMA)和镁安山岩/闪长岩类(MA):与洋俯冲作用相关的两类典型的火成岩类[J]. 中国地质, 37(4): 1 112~1 118.
- 付长亮,孙德有,张兴洲,等. 2010. 吉林浑春三叠纪高镁闪长岩的发现及地质意义[J]. 岩石学报, 26(4): 1 089~1 102.
- 龚全胜,刘明强,李海林,等. 2002. 甘肃北山造山带类型及基本特征[J]. 西北地质, 35(3): 28~34.
- 何世平,任秉琛,姚文光,等. 2002. 甘肃内蒙古北山地区构造单元划分[J]. 西北地质, 35(4): 30~40.
- 何世平,周会武,任秉琛,等. 2005. 甘肃内蒙古北山地区古生代地壳演化[J]. 西北地质, 38(3): 6~15.
- 黄华,高山,胡兆初,等. 2007. 辽西彰武地区中生代高镁安山岩地球化学及其对新生下地壳拆沉作用的指示[J]. 中国科学(D辑), 37(10): 1 287~1 300.
- 李承东,张福勤,苗来成,等. 2007. 吉林色洛河晚二叠世高镁安山岩SHRIMP锆石年代学及其地球化学特征[J]. 岩石学报, 23(4): 767~776.
- 李锦铁,张进,杨天南,等. 2009. 北亚造山区南部及其毗邻地区地壳构造分区与构造演化[J]. 吉林大学学报(地球科学版), 39(4): 584~605.
- 李玮,陈隽璐,董云鹏,等. 2016. 早古生代古亚洲洋俯冲记录:来自东天山卡拉塔格高镁安山岩的年代学、地球化学证据[J]. 岩石学报, 32(2): 505~521.
- 李小波,王保弟,刘函,等. 2015. 西藏达如错地区晚侏罗世高镁安山岩-班公湖-怒江洋壳俯冲消减的证据[J]. 地质通报, 34(2/3): 251~261.
- 刘雪亚,王荃. 1995. 中国西部北山造山带的大地构造及其演化[J]. 地学研究, 28(1): 37~48.
- 孟贵祥,吕庆田,严加永,等. 2009. 北山内蒙古地区铁矿成矿特征及其找矿前景[J]. 矿床地质, 28(6): 815~829.
- 彭松柏,刘松峰,林木森,等. 2016. 华夏早古生代俯冲作用(II):大西洋高镁-镁质安山岩新证据[J]. 地球科学, 41(6): 931~947.
- 孙立新,张家辉,任邦方,等. 2017. 北山造山带白云山蛇绿混杂岩的地球化学特征、时代及地质意义[J]. 岩石矿物学杂志, 36(2): 131~147.
- 唐功建,王强. 2010. 高镁安山岩及其地球动力学意义[J]. 岩石学报, 26(8): 2 495~2 512.
- 王晓蕊,高山,柳小明,等. 2005. 辽西四合屯早白垩世义县组高镁安山岩的地球化学:对下地壳拆沉作用和Sr/Y变化的指示[J]. 中国科学(D辑), 35(8): 700~709.
- 武鹏,王国强,李向民,等. 2012. 甘肃北山地区牛圈子蛇绿岩的形成时代及地质意义[J]. 地质通报, 31(12): 2 032~2 037.
- 巫祥阳,徐义刚,马金龙,等. 2003. 鲁西中生代高镁闪长岩的地球化学特征及其成因探讨[J]. 大地构造与成矿学, 27(3): 228~236.
- 徐学义,何世平,王洪亮,等. 2008. 中国西北部地质概论-秦岭、祁连、天山地区[M]. 北京: 科学出版社, 1~347.
- 杨合群,李英,李文明,等. 2008. 北山成矿构造背景概论[J]. 西北地质, 41(1): 22~28.
- 杨合群,李英,赵国斌,等. 2010. 北山蛇绿岩特征及构造属性[J]. 西北地质, 43(1): 26~36.
- 杨合群,赵国斌,李英,等. 2012. 新疆-甘肃-内蒙古衔接区古生代构造背景与成矿的关系[J]. 地质通报, 31(2~3): 413~421.
- 尹继元,袁超,孙敏,等. 2012. 新疆哈图早二叠世富镁闪长岩的时代、地球化学特征和可能的成因机制[J]. 岩石学报, 28(7): 2 171~2 182.
- 张旗,钱青,翟明国,等. 2005. Sanukite(赞岐岩)的地球化学特征、成因及其地球动力学意义[J]. 岩石矿物学杂志, 24(2): 117~125.
- 张元元,郭召杰. 2008. 甘新交界红柳河蛇绿岩形成和侵位年龄的准确限定及大地构造意义[J]. 岩石学报, 24(4): 803~809.
- 赵振华,王强,熊小林,等. 2007. 新疆北部的富镁火成岩[J]. 岩石学报, 23(7): 1 696~1 707.
- 左国朝,刘义科,刘春燕. 2003. 甘新蒙北山地区构造格局及演化[J]. 甘肃地质学报, 12(1): 1~15.